Lasers Med Sci (2015) 30:165–172
DOI 10.1007/s10103-014-1618-0

ORIGINAL ARTICLE

Laser irradiation of ferrous particles for hyperthermia as cancer therapy, a theoretical study

Jigar M. Patel · Cahit A. Evrensel · Alan Fuchs · Joko Sutrisno

Received: 31 December 2013 / Accepted: 11 June 2014 / Published online: 1 August 2014

Abstract Our recent *in vivo* animal studies showed the feasibility of using micron sized iron particles to induce physical damage to breast cancer tumors and thereby triggering a localized immune response to help fight the cancer. Combining a hyperthermic treatment with this ongoing study may enhance the immune response. As a result, a novel treatment of inducing hyperthermia using iron particles excited by a continuous wave near-infrared laser was analyzed. In this theoretical study, Mie scattering calculations were first conducted to determine the absorption and scattering efficiencies of the suspended drug coated particles. The resulting heat transfer between the particles and the surrounding tumor and the healthy tissue was modeled using Pennes' Bioheat equation. Predicted temperature changes were satisfactory for inducing hyperthermia (42 °C), thermally triggering drug release, and even thermal ablation (55 °C).

Keywords Laser-tissue interaction · Hyperthermia

J. M. Patel (✉) · C. A. Evrensel (✉)
Department of Mechanical Engineering, University of Nevada, Reno, Reno, Nevada, 89557, USA
e-mail: jpatel2107@icloud.com
e-mail: cahit@unr.edu

A. Fuchs · J. Sutrisno
Department of Chemical Engineering, University of Nevada, Reno, Reno, Nevada, 89557, USA

J. Sutrisno
Chemical Engineering, University of Surabaya, Surabaya, 60223, East Java, Indonesia

Introduction

Recent study by the World Health Organization reported that the incidence rates of cancer are expected to grow by 75 % in the year 2030, with breast cancer being one of the seven most commonly occurring cancers [6]. Traditional methods of cancer treatment lead to killing of the tumor cells along with immune effector cells [16]. Eventually, the tumors metastasize to other organs with little to no resistance from the immune system. Our recent studies investigated the injection of micron sized iron particles into the tumor followed by an application of a permanent magnetic field to induce physical damage, and thereby triggering a localized immune response [5, 16]. This treatment resulted not only in suppression of tumor growth on the treated primary side, but also on the untreated contralateral side indicating a possible immune response.

This treatment can be further supplemented by a hyperthermia treatment, since raising the internal temperature of the tumor above 42 °C slowly starts killing the tumor cells and possibly enhancing the immune response [18]. Many researchers are actively studying the temperature effects of using gold nanoparticles or nanoshells excited by a near infrared (NIR) laser. The most relevant technique for this research is using the lasers to heat tumors in the range of hyperthermia to thermal ablation [20, 30]. The advantages of using gold nanoparticles (GNPs) are due to their strong absorption properties (a bulk surface plasmon resonance that is in the visible part of the electromagnetic spectrum), biocompatibility, and ease of conjugation to proteins and antibodies [41]. The GNPs are irradiated with pulsed laser beams, where the laser pulsing frequency is chosen to be greater than the GNP thermal relaxation frequency. This results in thermal confinement within the particle instead of heat being diffused away to the surrounding tissue. Thermal

confinement is important since it yields a localized thermal response, which is important for inducing damage before heat is dissipated to the surrounding medium. Rapid laser pulsing results in shock waves and high local pressure propagating in the medium. Such high temperatures can cause explosive vaporization of the fluid surrounding the GNPs or iron oxide particles [27, 29, 30]. Therefore, increasing the laser power can result in thermal responses ranging from thermal expansion to fragmentation of the particle.

Instead of introducing GNPs to our tumor models, it is proposed to utilize the micron sized iron particles used in our recent study [5, 16]. The laser treatment will be used to thermally release the coated anti-tumor drugs, induce hyperthermia, and thereby improve the immune response [9, 31, 40]. In this paper, the focus is on inducing hyperthermia, in particular, laser-particle and laser-tissue interactions, since the temperatures needed for hyperthermia represent the upper bound of the thermally controlled drug release. We analyze the use of continuous wave (CW) lasers to heat these iron particles in order to prevent thermal ablation and to provide a controlled heating environment. The resulting heat transfer between the particles and the surrounding tissue is modeled using the Pennes' Bioheat equation [1–3, 11, 19, 23]. The particles are assumed to be evenly distributed prior to heating with the laser. Once this treatment is complete, the particles can be excited by the permanent magnet to cause physical damage. With this assumption, the effects of magneto-optics, such as Kerr and Faraday rotations in the presence of magnetized particles, can be neglected.

Dynamic modeling

Light interacts with a particle by causing resonant oscillations of the free electrons in the metal; this resonance is described as surface plasmon resonance (SPR). When a laser is directed at a particle, the energy is absorbed by the free electrons in the metal (electron heating), which then raises the temperature of the particle (electron-phonon coupling), and finally the heat is transferred to the surrounding tissue (phonon-phonon coupling) [25, 30]. This heat generation is typically referred to as SAR, or the Specific Absorption Rate. For applications involving lasers, SAR is linearly dependent on the particle concentration, laser irradiance, and the absorption properties of iron particles. Mie theory was used to predict the scattering properties of the iron particles with an average radius of $4 \pm 2\ \mu$m. Elastic scattering was assumed to simplify the calculation process considerably without decreasing the validity of the solution [38]. Once the SAR value was obtained, it acted as a source term in the heat equation. By assuming a uniform distribution of iron particles inside the tumor, the temperature rise inside the tumor and the surrounding healthy tissue is predicted by the Pennes' Bioheat equation [1–3, 11, 19, 23].

Laser-particle interaction

As the electromagnetic wave propagates through the particle, the motion of the wave is dependent on the material properties and can be described by the refractive index, $m = \sqrt{\mu_r \epsilon_r}$, where μ_r and ϵ_r represent the relative permeability and permittivity, respectively [4, 17, 21, 24]. In the presence of dispersion, both the permeability and permittivity should be treated as frequency dependent. The permittivity as a function of the field frequency can be written as, $\epsilon_r(\omega) = \epsilon'(\omega) + i\epsilon''(\omega)$, commonly referred to as the complex dielectric constant. Kramers-Kronig Relations can be used to relate the real and imaginary parts to each other [1] in order to show that the dispersive and absorptive properties of the metal are not independent [26]. Unlike $\epsilon_r(\omega)$, $\mu_r(\omega)$ ceases to be meaningful at low frequencies [2] and therefore it can be set to unity [26]. Furthermore, the refractive index can be written in a complex form to distinguish between an absorbing (iron) and a non-absorbing (tissue) medium. The complex refractive index can be written as $m = n + i\kappa$, where n indicates the refraction of light, and κ is related to absorption. As expected, both n and κ can be expressed in terms of the real and imaginary parts of the complex dielectric constant [26]. Some authors prefer to use a negative sign instead, as in $m = n - i\kappa$ [21, 24]. It should be noted that these two definitions are complex conjugates of one another, but $\kappa > 0$ always represents a damped wave, i.e. an absorbing medium. Experimentally derived values of n and κ with respect to frequency were used to study the optical properties of iron particles [28].

The optical properties of particles can be calculated in terms of their scattering and absorption efficiencies as a function of the particle radius, a, refractive index, m, and the incident wavelength, λ. Mie total extinction, Q_{ext}, scattering, Q_{sca}, and absorption, Q_{abs}, efficiencies for a homogeneous sphere are,

$$Q_{ext} = \frac{2}{x^2}\sum_{n=1}^{\infty}(2n+1)\,\mathrm{Re}(a_n + b_n) \tag{1a}$$

$$Q_{sca} = \frac{2}{x^2}\sum_{n=1}^{\infty}(2n+1)\left(a_n^2 + b_n^2\right) \tag{1b}$$

$$Q_{abs} = Q_{ext} - Q_{sca} \tag{1c}$$

[1] $\epsilon''(\omega)$ has an additional term of conductance divided by the field frequency, σ/ω, since the material is a metal.

[2] It is meaningful in the range where the wavelength of oscillation is much greater than the atomic dimension of the material.

where a_n and b_n are scattering coefficients given by [4, 21, 24],

$$a_n = \frac{[D_n(mx)/m + n/x]\psi_n(x) - \psi_{n-1}(x)}{[D_n(mx)/m + n/x]\zeta_n(x) - \zeta_{n-1}(x)} \quad (2a)$$

$$b_n = \frac{[mD_n(mx) + n/x]\psi_n(x) - \psi_{n-1}(x)}{[mD_n(mx) + n/x]\zeta_n(x) - \zeta_{n-1}(x)}. \quad (2b)$$

Here, x is the size parameter (ratio of the meridional circumference of the scattering sphere to the wavelength of light in the scattering medium, $2\pi a/\lambda$), ψ_n and ζ_n are the Riccati-Bessel functions, and D_n is the logarithmic derivative equal to $\frac{d}{d(mx)} \log \psi_n(mx)$ [13]. The inclusion of the logarithmic derivative is strictly to reduce the numerical computation time. These scattering coefficients better help predict the absorption and scattering behavior of the injected ferrous particles based on the particle radius and refractive index. There are two additional scattering coefficients, c_n and d_n, which are related to the components of the electric and magnetic fields. However, these were neglected since both a_n and b_n modes dominate d_n and c_n modes respectively [4, 21, 24, 34]. In addition, there is also radiation pressure acting on each particle. When the photons strike the particle, there is a momentum transfer and they exert a force in the direction of propagation. With the particles suspended inside the tissue, this force is quite minimal in comparison with the restoring viscoelastic force acting on the particle and can be neglected.

It is important to note that the scattering coefficients presented above are only valid for an uncoated homogenous spherical particle. The iron particles considered in this study were coated with poly(N-isopropylacrylamide), whose thickness varied between 50 - 100 nm. DeRosa et al. investigated phase separations of P(NIPAm) solutions and gels using a NIR laser [12]. The absorbance of water alone and P(NIPAm) was fairly close, and the relative refractive index of P(NIPAm) and the surrounding water was 1. Since the refractive index of the tumor is similar to that of water, the scattering coefficients of a coated sphere would simply reduce to Eqs. 2a and 2b.

Laser-tissue interaction

Before the incident light can interact with the suspended iron particles, it will interact with both the tissue and surrounding air at the air-tissue interface. When irradiating the tissue with light, either the light is reflected or refracted, and the refracted light is either absorbed or transmitted through the tissue. Since tissue is a heterogeneous material with multiple layers, modeling tissue optics is very difficult. By assuming each layer is homogeneous and has isotropic properties, this non-linear problem can be simplified by analyzing the absorbing and scattering properties of

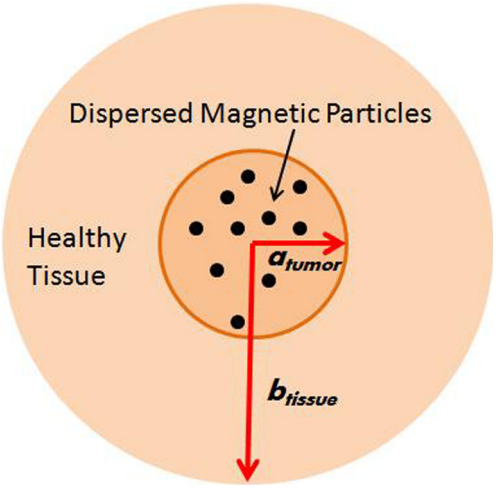

Fig. 1 Heat transfer geometry for simulation

the chromophores present in the tissue. A majority of chromophores inside the tumor or tissue can be broken down into three categories: water, oxyhemoglobin, and deoxyhemoglobin. By minimizing their absorbance, the suspended particles have a higher probability of absorbing the scattered light. Between 600 nm - 1300 nm, these chromophores display very low absorbance with maximum laser penetration depth. As a result, this range of wavelength is referred to as the optical biological window [7, 30, 36, 37]. Many researchers have experimentally found the breast tissue and tumor to be dominated by forward scattering, and having a low absorbance ($\kappa \sim 0$) with a refractive index, m_{tumor}, to be 1.33 ± 0.05 [8, 10, 14, 20, 32, 33, 36].

After the photon makes its way through the highly scattering media and excites the particle, the final stage of relaxation process is the energy transfer between the hot electron-phonon system and the tumor. Since the Biot number (ratio of the conduction resistance within the body to the convection resistance at the surface of the body, $\sim ha/k$) of an iron spherical particle surrounded by water is much less than 0.1, temperature can be assumed uniform throughout the particle. Heat transfer between the tissue and the particles was modeled using the Pennes' Bioheat equation. The model geometry in this study was considered to be of a 1 cm tumor surrounded by an infinite region of healthy tissue (Fig. 1).

The equations governing the temperature distribution in the domain considered can be written as,

$$\rho_1 c_1 \frac{\partial T_1}{\partial t} = \frac{k_1}{r^2}\frac{\partial}{\partial r}\left(r^2 \frac{\partial T_1}{\partial r}\right) - w_b c_b (T_1 - T_b) + q_m + \text{SAR} \quad \text{for } 0 < r < a_{tumor} \quad (3a)$$

$$\rho_2 c_2 \frac{\partial T_2}{\partial t} = \frac{k_2}{r^2}\frac{\partial}{\partial r}\left(r^2 \frac{\partial T_2}{\partial r}\right) - w_b c_b (T_2 - T_b) + q_m \quad \text{for } a_{tumor} < r < b_{tissue} \quad (3b)$$

Table 1 Thermal properties of Iron and Tissue

	Iron	Tissue
Thermal conductivity, k [W/(m·K)]	80.4	0.567
Density, ρ [kg/m^3]	7.87E+03	1050
Specific heat, c_p [kJ/(kg·K)]	0.45	1.5
Thermal diffusivity, α [m^2/s]	2.3E-05	1.5E-07

where ρ, c, T, k, and w are the density, specific heat, temperature, thermal conductivity, and volumetric blood perfusion rate, respectively. Subscripts 1, 2, and b refer to the tumor, surrounding tissue, and blood in both media, respectively. Additionally, q_m is the metabolic heat rate ($\sim$33800 W/m^3 [11]), a_{tumor} is the tumor radius, b_{tissue} is the surrounding tissue radius, and r is the distance from the center of the tumor [3, 11]. Some of the thermal properties used for the numerical simulations are given in Table 1.

The temperature at the center of the tumor was assumed to be finite, i.e. $|T_1(0,t)| < \infty$. Additionally, continuity condition at the boundary of the tumor and the tissue is enforced, such that $T_1(a_{tumor},t) = T_2(a_{tumor},t)$, and $k_1\frac{\partial T_1}{\partial r}(a_{tumor},t) = k_2\frac{\partial T_2}{\partial r}(a_{tumor},t)$. Also, the temperature at the boundary of the healthy tissue was the normal body temperature T_0, which was also the temperature used for the initial condition across both boundaries, i.e. $T_2(b_{tissue},t) = T_1(r,0) = T_2(r,0) = T_0$ [3]. The Specific Absorption Rate is given by,

$$\mathrm{SAR} = N \cdot C_{abs} \cdot I \tag{3c}$$

where N is the particle concentration (number of particles/m^3), C_{abs} is the absorption cross section calculated by multiplying the absorption efficiency, Q_{abs}, with the scattering area of the particle, πa^2, and I is the incident irradiance (W/m^2). Equations 3a and 3b were solved numerically using COMSOL for a NIR laser an average irradiance of 4 W/cm^2 at 820 nm wavelength.

Results

The iron particles chosen for this study were 8 ± 4 μm in diameter due to a Gaussian distribution. Since the particles are suspended inside the tumor, the relative wavelength, $\lambda_r = \lambda_{incident}/m_{tumor}$, was used for Mie calculations and the resulting solution is shown Fig. 2. Varying the refractive index of the tumor had very little effect on the efficiency values. For example, at 4 μm, 0.05 error in the tumor refractive index resulted in an error of 0.012 and 0.008 for scattering and absorption efficiencies, respectively. However, as the particle radius increased, all three efficiencies decreased and approached asymptotic values. Thus, in order to have the highest absorption efficiency, smaller particles must be

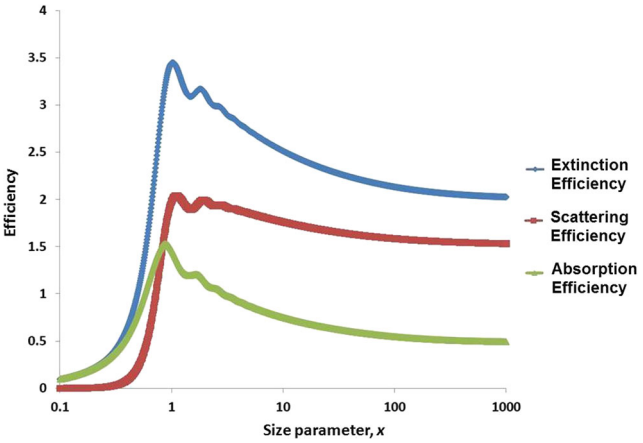

Fig. 2 Efficiency calculations for an iron particle with varying size parameter (log-scale) for m_{tumor} = 1.33 and $\lambda_{incident}$ = 820 nm. For $a = 4\mu$m and λ_r = 616.5 nm, $x \approx 41$ with an absorption efficiency of 0.601

used. There is only one maximum in Q_{ext} in the Fig. 2 above, which shifts to smaller x with increasing κ with only a few minor oscillations in the beginning. These oscillations are governed by the resonant electromagnetic normal modes in a sphere due to the denominators of a_n and b_n being minimum [4, 34]. In practical applications, this would be hard to observe in polydispersions, but it does show the effect the absorption coefficient has on damping this resonant behavior. Comparing these to efficiency calculations for a gold particle in Fig. 3, the absorption for iron is definitely greater, as shown in Fig. 2. Max absorption for GNPs occurs at lower wavelengths, typically outside the optical biological window [30]. As a result, by using core-shell gold nanoparticles, it is possible to tune the SPR of the particle to obtain the highest absorption at the desired wavelength by varying the core-to-shell ratio [22]. Hence, instead of using just

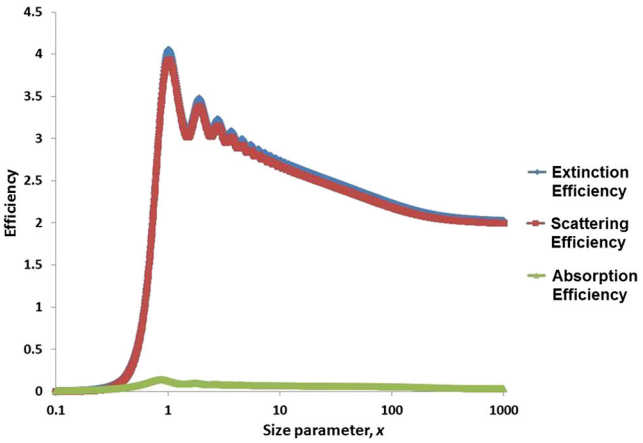

Fig. 3 Efficiency calculations for a gold particle with varying size parameter (log-scale) for m_{tumor} = 1.33 and $\lambda_{incident}$ = 820 nm

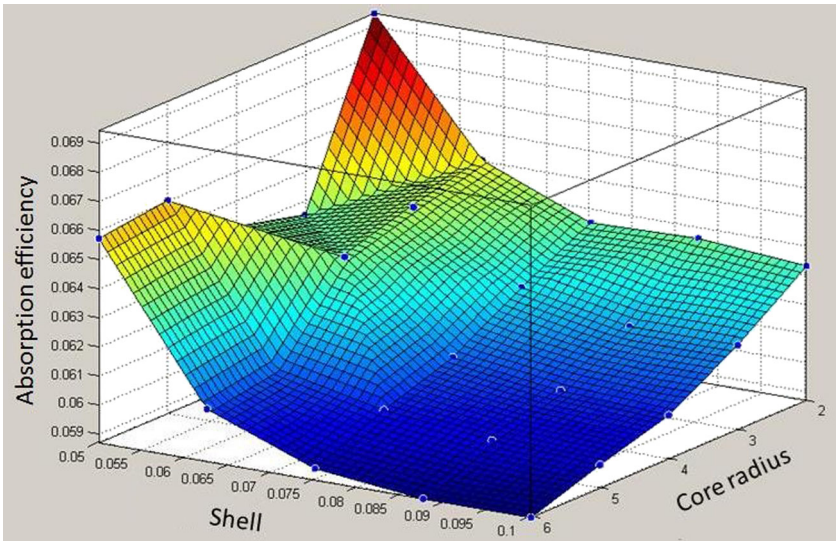

Fig. 4 Absorption efficiency for a varying core (Fe) and shell (Au) with $m_{tumor} = 1.33$ and $\lambda_{incident} = 820$ nm. Both the core radius and shell thickness are shown in units of μm

plain gold nanoparticles for this type of hyperthermia application, nearly all researchers resort to using these core-shell nanoparticles. Some researchers have coated iron oxide particles with gold for biomedical applications [35]. The gold shell thickness was varied in the same range as P(NIPAM), from 50 - 100 nm as shown in Fig. 4. Our results indicated that there was no possible advantage in coating the iron particles with gold, and it lowered absorption efficiency by an order of magnitude. Even lowering the core-shell size in the few nanometer range did not increase the absorption efficiency. However, the benefit of using these large particles lies in their scattering direction. One of the biggest challenges in treatment of tumors using this technique is laser depth penetration. Since the radius of the particles is bigger than the wavelength, scattering involves higher orders of the angular functions, resulting in a more forward directed scattering, and thus a deeper light penetration. This can be shown by the asymmetry parameter, $\langle \cos\theta \rangle$. Averaging the asymmetry parameter is simply the result of an average deflection angle. It vanishes if the scattering is isotropic, but it is positive if more light is scattered in the forward direction and negative if scattering is backwards [4]. In Fig. 5, $\langle \cos\theta \rangle < 0$ for a particle radius of 66 nm for iron, 112 nm for gold, and 104 nm for the gold nanoshell. For particle sizes below these numbers, backward scattering will be favored. Most hyperthermic applications use gold nano particles or nanoshells below these size limits [30]. The tissue is already forward scattering; however, it can be argued that using these large particles ensures we generate similar internal temperatures by scattering the incident light deeper into the cancerous tumor.

Pennes' Bioheat Eqs. 3a and 3b were solved numerically to predict the temperature changes in the tumor (1 cm) and the surrounding medium (4 cm). As with most problems of such type, the surrounding medium was assumed to be infinite in nature with the boundary temperature fixed at $T_0 = 37$ °C. Healthy tissues typically respond to hyperthermia by increasing the blood perfusion rate, and sometimes even exceeding the normal healthy rate by an order of magnitude [38]. However, once the heating stresses the tissue, vascular stasis occurs and the blood perfusion drops. Hence, this model can be studied by taking a small perturbation around the mean value for blood perfusion [11]. But the tumor consists of a leaky vasculature and the increase in blood perfusion is quite small. Thus, the perturbation method was ignored, and two values representing a mean average (1 kg/m^{3}s) and a maximum (5 kg/m^{3}s) were numerically investigated, as shown in Fig. 6. The characteristic time of the transient process, $\tau_{macro} = \frac{a^2_{tumor}}{\alpha} \sim 160$ s,

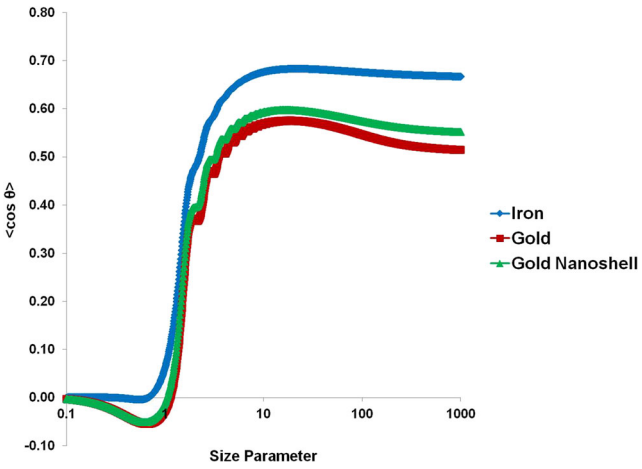

Fig. 5 Asymmetry vs. size parameter (log-scale) for $m_{tumor} = 1.33$ and $\lambda_{incident} = 820$ nm. The plot was constructed using refractive indices for iron and gold [28]; whereas, the dielectric function was used for the gold nanoshell with an inner and outer radius of 20 nm and 25 nm, respectively [15]

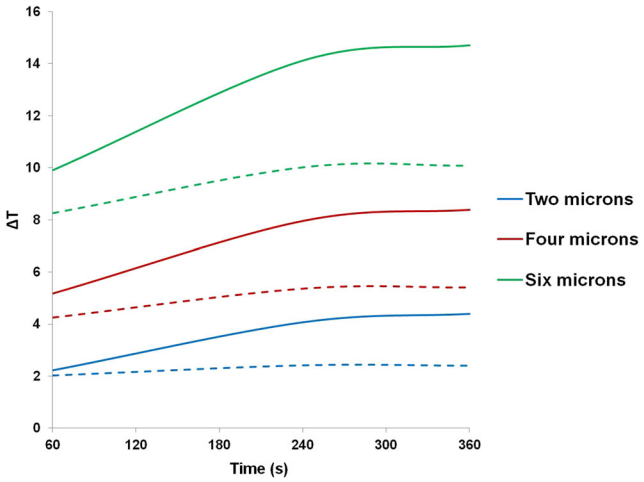

Fig. 6 ΔT (K) vs Time (s) for $N = 2.85 \times 10^{11}$ particles/m^3, and $I_0 = 4$ W/cm^2. *Solid lines* represent a blood perfusion rate of 1 kg/m^{3}s, and the *dotted lines* represent a blood perfusion rate of 5 kg/m^{3}s for the same conditions. Simulations are shown for 60 s and above to note the net temperature rise between the blood perfusion rates at the smallest particle size

provided a good estimate on the time needed to reach 2/3 of the steady state temperature [23]. The concentration, N, and the radius of the particles, a were varied to see their effects on the steady state temperature, as shown in Fig. 7. The blood perfusion rate, w_b, the concentration, N, and the radius of the particles, a, were varied to see their effects on the steady state temperature. Increase in the blood perfusion rate decreased the maximum temperature considerably; whereas, an increase in both the particle concentration and radius resulted in a higher net temperature. It is important to note that even though the value taken from the literature for the metabolic heat rate may not be very accurate

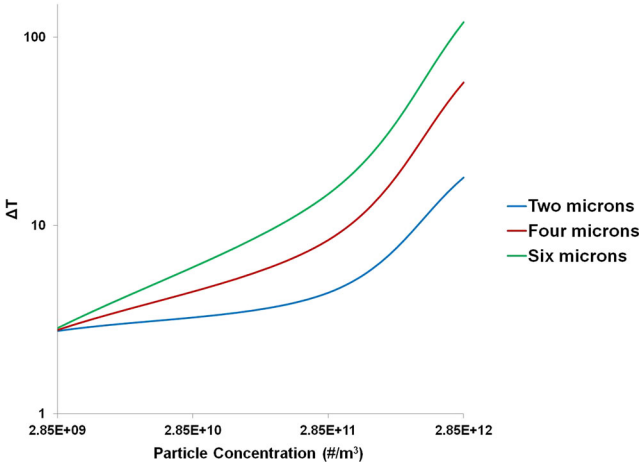

Fig. 7 ΔT (K) (log-scale) vs. Particle Concentration (#/m^3) (log-scale) for varying particle radius shown at $t = 360$ s and $I_0 = 4$ W/cm^2

[11], its contribution is small compared to the dominating source term in the Pennes' Bioheat equations. In comparison, neglecting the metabolic heat rate completely results in a maximum of 10 % difference for ΔT at the source origin. This difference is further reduced with the increasing radial distance away from the heat source.

Throughout this study, the term irradiance has been used to define the incident radiation. By definition, irradiance is the rate of energy delivered per second per unit area of the tissue surface, and for CW radiation, this is the most applicable definition. Fluence rate has the same units as irradiance, but is representative of the radiation over all directions, since an absorber inside the tissue will encounter radiation scattering off of multiple directions. Using experimental data for absorption and reduced scattering properties of breast tissue and tumors, Beer's law was modified to obtain an average fluence rate of 2.01 W/cm^2 where it attenuated by a factor of e^{-1} at ~7 mm tissue depth, and the resulting temperature changes are given in Table 2 [8, 33, 38]. Clearly, a decrease in the incident radiation yields a decrease in the SAR, and thus a decrease in the max temperature increase. However, there is a significant problem with this analysis. Studies have shown that the backscattered light emerging from deep tissue raises the irradiance right below the surface of the skin, and amplifies the incident irradiation by 140 % [20, 38, 39]. This is the reason why most *in vivo* studies report highest temperature gains ~1 mm below the apical surface. Regardless of the irradiance, experimental results show thermal damage spanning a depth of several millimeters to even 1 cm. This depth can be increased with a higher laser irradiance, and lowering the particle concentration to allow for further light penetration [7, 20, 30, 38]. An argument could be made that the aforementioned heat transfer model is not accurate enough to account for these changes. However, tumor and tissue properties vary for each individual based on fat content, muscle density, etc, and due to this non-linearity, only approximations can be modeled at best.

Table 2 Max ΔT (K) for varying blood perfusion rate, w_b, and concentration, N, with a constant irradiance of 2.01 W/cm^2, particle radius, a, equal to 4 μm for simulation times t equal to 60, 240, 360 seconds

		ΔT_{max}		
w_b (kg/m^{3}s)	N (#/m^3)	60 s	240 s	360 s
1	2.85E+09	1.194	2.755	2.766
1	2.85E+11	3.227	5.392	5.751
1	2.85E+12	22.460	30.324	31.493
5	2.85E+09	0.916	1.343	1.317
5	2.85E+11	3.053	3.385	3.384
5	2.85E+12	18.923	22.323	22.504

Conclusion

The purpose of this theoretical study was to investigate the use of iron particles, instead of GNPs, excited by a continuous wave near-infrared laser for inducing hyperthermia to enhance previously proposed cancer therapy using similar particles. The results showed that the efficiencies of the micron sized iron particles were large enough for inducing hyperthermia, triggering possible drug release, and in high concentrations, even thermal ablation. Both the absorption and scattering efficiencies of the particles decreased with an increasing particle radius to an asymptotic value. While preparing the iron particles for *in vivo* studies, oxide coating may be unavoidable. Although the coating may reduce the absorption efficiency in the NIR range, this effect could be accounted for by using a higher concentration of particles. Core-shell method typically used in GNPs was shown to have no beneficial effect on the iron particles, thus indicating a need for a detailed SPR analysis in order to maximize the absorption efficiency. Laser penetration depth is predicted to be about $\sim$7 mm, or where the fluence rate had attenuated by a factor of e^{-1}, for human tissue. In contrast to the GNPs, micron sized iron particles were shown to be dominated by forward scattering, which would result in two major advantages: thermal damage spanning on the order of centimeter or more, and absence of the high temperatures observed while using gold nanoshells $\sim$1 mm below the surface, thus providing a more controlled heating environment. However, these theoretical simulations still need to be supplemented with experimental results. Penetration depth may be increased for treating deeply embedded tumors by either lowering the particle concentration or increasing the incident irradiation.

References

1. Andrà W, d'Ambly C, Hergt R, Hilger I, Kaiser WA (1999) Temperature distribution as function of time around a small spherical heat source of local magnetic hyperthermia. J Magn Magn Mater 194:197–203
2. Atkinson WJ, Brezovich IA, Chakraborty DP (1984) Usable frequencies in hyperthermia with thermal seeds. IEEE Trans BME Biomed Eng 31(1):70–75
3. Bagaria HG, Johnson DT (2005) Transient solution to the bioheat equation and optimization for magnetic fluid hyperthermia treatment. Int J Hyperth 21(1):57–75. doi:10.1080/02656730410001726956
4. Bohren CF, Huffman DR (1983) Absorption and scattering of light by small particles. Wiley
5. Bouchlaka MN, Sckisel GD, Wilkins D, Maverakis E, Monjazeb AM, Fung M, Welniak L, Redelman D, Fuchs A, Evrensel CA, Murphy WM (2012) Mechanical disruption of tumors by iron particles and magnetic field application results in increased anti-tumor immune responses. PLoS ONE 7(10). doi:10.1371/journal.pone.0048049
6. Bray F, Jemal A, Grey N, Ferlay J, Forman D (2012) Global cancer transitions according to the Human Development Index (2008–2030): a population-based study. The Lancet Oncology. doi:10.1016/S1470-2045(12)70211-5. in Press
7. Byrnes KR, Waynant RW, Ilev IK, Wu X, Barna L, Smith K, Heckert R, Gerst H, Anders JJ (2005) Light promotes regeneration and functional recovery and alters the immune response after spinal cord injury. Lasers Surg Med 36(3):171–185
8. Cerussi A, Shah N, Tromberg B, Hsiang D, Butler J, Durkin A (2006) Electromagnetic scattering by magnetic spheres. J Biomed Opt 11(4)
9. Cippitelli M, Fionda C, Di Bona D, Piccoli M, Frati L, Santoni A (2005) Hyperthermia enhances CD95-ligand gene expression in T lymphocytes. J Immunol 174(1):223–232
10. Cubeddu R, Pifferi A, Taroni P, Torricelli A, Valentini G (1999) Noninvasive absorption and scattering spectroscopy of bulk diffusive media: An application to the optical characterization of human breast. Appl Phys Lett 74(6):874–876
11. Deng ZS, Liu J (2001) Blood perfusion-based model for characterizing the temperature fluctuation in living tissues. Physica A: Statistical Mechanics and its Applications, vol 300
12. DeRosa ME, DeRosa RL, Noni LM, Hendrick ES (2007) Phase separation of poly(N-isopropylacrylamide) solutions and gels using a near infrared fiber laser. J Appl Polym Sci 105(4):2083–2090
13. Du H (2004) Mie-Scattering Calculation. Appl Opt 43(9):1951–1956
14. Durduran T, Choe R, Culver J, Zubkow L, Holboke M, Giammarco J, Chance B, Yodh A (2002) Bulk optical properties of healthy female breast tissue. Phys Med Biol 47:2847–2861
15. Erickson TA, Tunnell JW (2007) Gold nanoshells in biomedical applications. Wiley-VCH Verlag GmbH & Co. KGaA
16. Evrensel C, Fuchs A, Gordaninejad F, Patel J, Sutrisno J, Nation C, Cook C, Rosen A, Bouchlaka M, Murphy W (2011) Immunotherapy with magnetorheologic fluids. Era of hope
17. Hapke B (2005) Theory of reflectance and emittance spectroscopy, 1st edn. Cambridge University Press
18. Hergt R, Dutz S, Mùller R, Zeisberger M (2006) Magnetic particle hyperthermia: nanoparticle magnetism and materials development for cancer therapy. J Phys Condens Matter 18(38):S2919
19. Hilger I, Hergt R, Kaiser WA (2005) Towards breast cancer treatment by magnetic heating. J Magn Magn Mater 293(1):314–319
20. Hirsch L, West J, Stafford R, Bankson J, Sershen S, Price R, Hazle J, Halas N (2003) Nanoshell-mediated near-infrared thermal therapy of tumors under magnetic resonance guidance. Proc Natl Acad Sci U S A 100(23):13,549–13,554
21. Hulst HVD (1957) Light Scattering by Small Particles. Wiley
22. Jain PK, Lee KS, El-Sayed IH, El-Sayed MA (2006) Calculated absorption and scattering properties of gold nanoparticles of different size, shape, and composition: applications in biological imaging and biomedicine. J Phys Chem B 110(14):7238–7248
23. Keblinski P, Cahill DG, Bodapati A, Sullivan CR, Taton T (2006) Limits of localized heating by electromagnetically excited nanoparticles. J Appl Phys:100
24. Kerker M (1969) The Scattering of Light and other electromagnetic radiation. Academic Press. Inc
25. Kittel C (2004) Introduction to solid state physics, 8th edn. Wiley
26. Landau L, Lifshitz E, Pitaevskiĭ L (1984) Electrodynamics of continuous media, vol 8, 2nd edn. Pergamon Press
27. Letfullin RR, Joenathan C, George TF, Zharov VP (2006) Laser-induced explosion of gold nanoparticles: potential role for nanophotothermolysis of cancer. Nanomedicine 1(4):473–480

28. Ordal MA, Long LL, Bell RJ, Bell SE, Bell RR, R W Alexander J, Ward CA (1983) Optical properties of the metals Al, Co, Cu, Au, Fe, Pb, Ni, Pd, Pt, Ag, Ti, and W in the infrared and far infrared. Appl Opt 22(7):1099–1119
29. Pitsillides CM, Joe EK, Wei X, Anderson RR, Lin CP (2003) Selective cell targeting with light-absorbing microparticles and nanoparticles. Biophys J 84(6):4023–4032. doi:10.1016/S0006-3495(03)75128-5
30. Qin Z, Bischof JC (2012) Thermophysical and biological responses of gold nanoparticle laser heating. Chem Soc Rev 41:1191–1217
31. Schueller G, Stift A, Friedl J, Dubsky P, Bachleitner-Hofmann T, Benkoe T, Jakesz R, Gnant M (2003) Hyperthermia improves cellular immune response to human hepatocellular carcinoma subsequent to co-culture with tumor lysate pulsed dendritic cells. Int J Oncol 22(6):1397–1402
32. Shah N, Cerussi A, Eker C, Espinoza J, Butler J, Fishkin J, Hornung R, Tromberg B (2001) Noninvasive functional optical spectroscopy of human breast tissue. Proc Natl Acad Sci 98(8):4420–4425
33. Srinivasan S, Pogue BW, Jiang S, Dehghani H, Kogel C, Soho S, Gibson J, Tosteson T, Poplack S, Paulsen K (2003) Interpreting hemoglobin and water concentration, oxygen saturation, and scattering measured in vivo by near-infrared breat tomography. Proc Natl Acad Sci U S A 100(21):12,349–12,354
34. Stratton JA (1941) Electromagnetic Theory. McGraw-Hill Book Company. Inc
35. Tamer U, Gündoğdu Y, Boyaci IH, Pekmez K (2010) Synthesis of magnetic core-shell Fe_3O_4-Au nanoparticle for biomolecule immobilization and detection. J Nanopart Res 12:1187–1196
36. Tromberg B, Shah N, Lanning R, Cerussi A, Espinoza J, Pham T, Svaasand L, Butler J (2000) Non-Invasive in vivo characterizatoin of breast tumors using photon migration spectroscopy. Neoplasia 2(1-2):26–40
37. Weissleder R (2001) A clearer vision for in vivo imaging. Nat Biotechnol:19
38. Welch AJ, van Gemert MJ (2011) Optical-thermal response of laser-irradiated tissue, 2nd edn. Springer
39. Welch AJ, Torres J, Cheong WF (1989) Laser physics and laser-tissue interaction. Tex Heart Inst J 16(3):141–149
40. Zhang HG, Mehta K, Cohen P, Guha C (2008) Hyperthermia on immune regulation: A temperature's story. Cancer Lett 271(2):191–204
41. Zharov VP, Letfullin RR, Galitovskaya EN (2005) Microbubbles-overlapping mode for laser killing of cancer cells with absorbing nanoparticle clusters. J Phys D Appl Phys 38:2571–2581